CREEP DEFORMATION OF STOICHIOMETRIC

URANIUM DIOXIDE SINGLE CRYSTALS

by

WILLIAM ROBERT STURROCK

A Thesis Submitted in Partial
Fulfilment of the Requirements
for the Degree of
Master of Applied Science

in the Department

of

METALLURGY

We accept this thesis as conforming to
the standard required from candidates
for the degree of Master of Applied Science

Members of the Department of Metallurgy

THE UNIVERSITY OF BRITISH COLUMBIA

February, 1962

ABSTRACT

Rectangular beams of high density single-crystal UO_2 were prepared from large grains of fused UO_2. They were deformed under constant load in four-point bending in hydrogen at temperatures from 1340 to $1420^\circ C$.

The results appear to fit a creep equation of the form

$$\dot{e} = C(\sigma_{max})^n_{SS} \exp(-Q/RT)$$

where

$\dot{e}$ = steady-state creep rate

$(\sigma_{max})_{SS} \equiv \tau_{\langle 011 \rangle}$ = resolved shear stress in $\langle 011 \rangle$ directions on $\{111\}$ planes

Q = 118 ± 23 kcal/mole

C = constant; and $3 < n < 4$

in the regions of stress and temperatures examined. Faint slip lines were observed.

ACKNOWLEDGEMENTS

TABLE OF CONTENTS

LIST OF ILLUSTRATIONS

LIST OF TABLES

I   INTRODUCTION

The Canadian nuclear power program is based on the use of uranium dioxide fuel and heavy water moderator. Natural uranium dioxide has many advantages as a nuclear fuel since it has a relatively low cost and is easily processed into high density shapes by powder metallurgical methods. It is isotropic and free from the low temperature phase changes of metallic uranium. However, its refractory nature and low thermal conductivity cause high thermal gradients which result in cracking and disintegration. Therefore, it would be desirable to know the effect of grain boundaries, grain size and density on the high-temperature ductility of polycrystalline material. This can of course be accomplished by examining the effect of changing these variables on polycrystalline specimens. But this approach is not without its difficulties since, if one changes grain size, the density changes as well, not to mention pore size and shape.

In the study of the plastic behaviour of metals, much has been learned from the testing of single crystals. Therefore, it was felt that in order to understand better the plastic behaviour of polycrystalline UO_2, an examination of single crystals would be of interest. To this end, this investigation has been concerned with the creep of single crystals of UO_2 at high temperatures. Specifically, the measurement of centre-point deflection rates of stoichiometric single crystals of UO_2 under constant load in bending at temperatures of $1340^{\circ}C$ to $1420^{\circ}C$ has been performed.

The results show that creep in bending involves slip on $\{111\}$ planes in the $\langle 110 \rangle$ directions, the rate depends on the resolved shear stress to the exponent n, where $3 < n < 4$, and the apparent activation energy is 118 ± 23 kilocalories for the overall creep process.

II   DEFORMATION AND CREEP IN CRYSTALLINE NON-METALS

Ceramists have long been interested in the mechanical properties
of refractory materials at all temperatures. However, recent requirements
for structures that will withstand temperatures far above the service limit
of metallic solids has stimulated research into the mechanical properties of
non-metallic solids at high temperatures for such diverse applications as
turbine components, re-entry cones and nuclear fuels.

Deformation studies at low temperatures (temperatures less than
approximately $\frac{1}{2}$ mp) are hindered by the inherent brittleness of non-metallic
materials. Problems such as specimen fabrication, gripping and porosity
which in the case of metallic materials are relatively minor in nature,
become serious obstacles in the testing of ceramic materials. Nonetheless,
the nature of the mechanical behaviour of ionic crystals at room temperature
is perhaps better understood than metal crystals because of, as pointed out
by J. J. Gilman[1], the relatively simple chemical binding in them and the
feasibility of direct observation of dislocations in the transparent ionic
crystals.

High temperature ($T > \frac{1}{2}$ mp) deformation studies on ceramic
materials, while experimentally no less difficult[2] have been more widely
performed since, in general, the ductility of ceramics increases with increas-
ing temperature. Much of the work has dealt with the time-dependent deform-
ation of ceramics; that is, the deformations produced under constant load
or constant stress, the former being the more common loading technique.
And since pure single crystals of ceramics, in particular refractory oxides,
have only recently been available, most of such creep studies have been
performed on polycrystalline materials. For example, Chang[3] has examined

the creep of polycrystalline Al_2O_3 and BeO and the effect of additions on the creep rate. Parr et al.[4] studied the creep of silicon nitride and silicon carbide, and Scott et al.[5] examined polycrystalline UO_2.

Tensile creep tests of long, thin sapphire single crystals have been performed by Wachtman[6] and he found that creep occurs by slip on the (0001) plane in the $[11\bar{2}0]$ direction.

III STRUCTURE OF UO$_2$

Uranium dioxide is a dark brown to black crystalline solid possessing the fluorite (CaF$_2$) structure shown in Figure 1, with a lattice
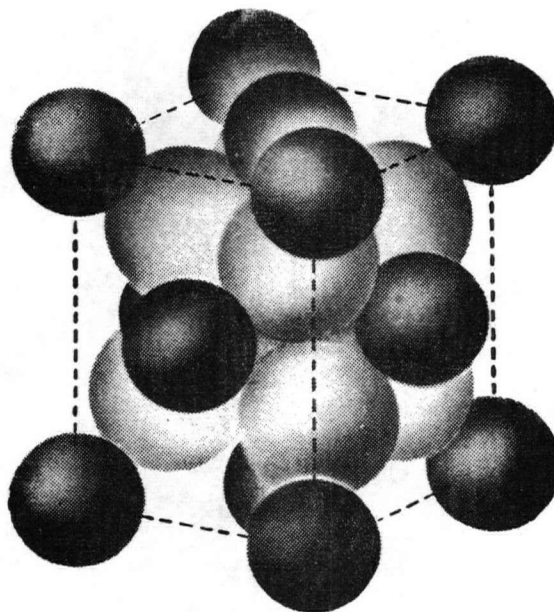
<u>Figure 1</u>   Fluorite type unit cell: (After Azaroff[7].)

parameter of 5.468 A$^{\circ}$ and theoretical density of 10.968 gm/cc at 26°C.[8] There are equivalent interstitial sites at the body centre and edge centres of the unit cell (U$_4$O$_8$) making a total of one interstitial site per uranium atom.[9] UO$_{2.0}$ will readily pick up oxygen above about 200°C to form stable U$_3$O$_8$. However, at room temperature, non-stoichiometric oxide will consist of the two phases UO$_{2+x}$ and U$_4$O$_9$.[10] There is also evidence that material solidified from the melt at 2800°C can exist as a single phase, with the fluorite structure, as UO$_{1.85}$[11]. The UO$_2$ - O phase diagram is in Appendix I.

IV PRIOR INVESTIGATIONS OF UO_2 DEFORMATION

A. Polycrystalline

As pointed out above, most of the work on refractory oxides has been done on polycrystalline materials, and UO_2 is no exception. One of the first such studies[12] examined the effect of particle size of fused UO_2 on the bulk density of sintered compacts and the flexural strength in 4-point bending at temperatures ranging from room temperature to $1000^{\circ}C$. The flexural strength was found to decrease with initial particle size, and to increase with test temperature, and the rate of change of strength with temperature decreases with increasing particle size and as the sintered density decreases.

Two investigations have been carried out recently using creep under 3-point bending at high temperatures. Scott, Hall and Williams[5] found that non-stoichiometric uranium dioxide deformed plastically at about $800^{\circ}C$, but that stoichiometric dioxide did not deform plastically under $1600^{\circ}C$. The creep rates for UO_{2+x} were found to obey the expression

$$\dot{e} = A \sinh \left(\frac{\sigma}{\sigma_0}\right) \exp \left(-Q/RT\right) \qquad (1)$$

where $\dot{e}$ is the strain-rate, σ the stress and T the absolute temperature. A and σ_0 are material constants. Values of Q are quoted as 65 kcal for $UO_{2.16}$, 72 kcal for $UO_{2.06}$ and $\geqslant$95 kcal for $UO_{2.00}$, per mole.

The second investigation by Armstrong, Irvine and Martinson[13] on stoichiometric UO_2 shows that $UO_{2.00}$ will deform plastically at $1250^{\circ}C$; the creep rate can be represented by the expression

$$\dot{e} = A \exp \left(-Q/RT\right)\sigma^n \qquad (2)$$

where $\dot{e}$ is the steady state strain rate, σ is the applied tensile stress
and A and n are material constants. They found that Q is 91 $\pm$ 8 kcal and
n = 1.0, for stresses below about 10,000 psi and for high density (93%
theoretical) material.

B.   Single Crystals

One other investigation[14] besides the present one, has under-
taken to use single crystals of UO_2. Small crystals were metallographically
polished and then deformed in compression at temperatures ranging from
700° to 1900°C. The most active slip plane at all temperatures was $\{100\}$,
with $\{110\}$ and $\{111\}$ becoming more active as the temperature was increased.

V   THEORY AND METHODS PERTINENT TO THIS INVESTIGATION

A.   Creep in Bending

By far the greatest amount of creep data have been obtained for metals from uniaxial tension tests under constant load. The time dependence of strain at constant temperatures of such a test is shown in Figure 2.
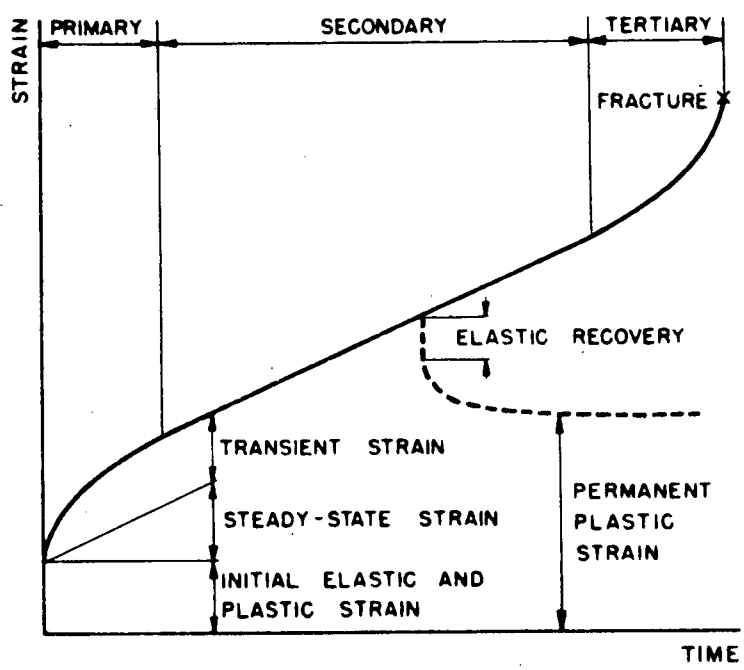
Figure 2   Schematic constant tensile load creep test at constant temperature. Dotted line shows behaviour if speciment is unloaded during test. (after Finnie[15])

The secondary stage of minimum strain rate may often be very prolonged and is the section most amenable to experimental study. At constant temperature, the steady-state strain rate is a function only of stress and may be represented by

$$\dot{e} = k \sigma^n \qquad (3)$$

where $\dot{e}$ is the strain rate, σ the stress, and k and n are material constants.

The temperature dependence of the strain rate may be represented by

$$\dot{e} = A \exp\left(-Q/RT\right) \tag{4}$$

where R is the gas constant, T the absolute temperature, and A a material constant. As pointed out by Dorn[16], Q , the observed activation energy, does not necessarily represent the activation energy for a single process, but may be an appropriately weighted average of the activation energies of all operative processes giving rise to creep.

The lower limit of temperature is, of course, determined by the smallest strain rate that can be detected; the upper limit being determined by the furnace components. In this case, that temperature range is about 1250°C to 1425°C. Specimens of constant rectangular cross-section have the most convenient shape to cut (since diamond abrasive wheels must be used) from the raw materials available. Therefore, bend, rather than say tensile, testing of prismatic beams of uniform cross-section was chosen for this investigation, and four-point loading was chosen over three-point loading for reasons outlined in Appendix II.

The simplification of the experimental problems by the use of bending in the place of tension, however, comes at a price. The experimentally measured quantities are only indirectly related to those of the tension test and several simplifying assumptions must be made.

An analysis of the use of bending to determine the precise tensile properties of ceramic bodies at room temperature has been given by Duckworth[17] and he recommends, on the basis of his analysis, that 4-point loading on a rectangular specimen with a reduced section for the gauge length should be used. He also recommends that strain should be

measured in both the upper and lower fibres, thus avoiding errors introduced by assumption 4 below.

The centre section of beam loaded in four-point bending has acting on it a constant bending moment. (See Appendix II.) Timoshenko's[18] analysis of creep in bending is briefly as follows:

First the following assumptions are made:

(1) Cross-sections remain plane;

(2) Each longitudinal fibre is in a condition of simple tension or compression;

(3) The creep equation (3) holds for tension and compression a considerable time after the load has been applied;

(4) Moduli in tension and compression are equal.

Then he shows that for a rectangular beam of width b and height h

$$(\sigma_{max})_{SS} = \frac{Mh}{2I} \left(\frac{2n+1}{3n}\right) \qquad (5)$$

where $(\sigma_{max})_{SS}$ = stress at the outer fibres in steady state

M = applied bending moment

n = exponent in equation (3)

I = moment of inertia about neutral axis.

Timoshenko then gives the differential equation of the deflection curve:

$$\frac{d^2y}{dx^2} = \pm \frac{2kt}{h} (\sigma_{max})^n_{SS} = \pm \frac{2kt}{h} \left(\frac{h}{2I}\right)^n \left(\frac{2n+1}{3n}\right)^n M^n \qquad (6)$$

where
y = deflection
x = distance along beam
h = height of beam
t = time
k = constant in equation (3)
n = exponent in equation (3)

In the case of a beam loaded in pure bending (M = const.) as is the centre section of a beam in four-point loading (see Appendix II), equation (6) can be integrated along the length of the beam (i.e. with respect to x) from x = 0 to x = m (where m is the length of the centre section) to give:

$$y = {}^+_- \frac{km^2}{h} (\sigma_{max})^n_{SS} t \qquad (7)$$

The deflection rate relative to the point of load application then is

$$\frac{dy}{dt} = \dot{y} = {}^+_- \frac{km^2}{h} (\sigma_{max})^n_{SS} \qquad (8)$$

The maximum strain in the outer fibres is given by

$$e_{max} = \frac{h}{2\rho} \qquad (9)$$

where ρ is the radius of curvature; the curvature and deflection (y) of a beam bent in a circular arc are related by

$$\rho \cong \frac{m^2}{8y} \qquad (10)$$

Combining equations (9) and (10), and differentiating with respect to time

$$\dot{e}_{max} = \frac{4h}{m^2} \dot{y} \qquad (11)$$

Then substitution of $\dot{y}$ in equation (8) yields

$$\dot{e}_{max} = {}^+_- 4k(\sigma_{max})^n_{SS} \qquad (12)$$

The elastic maximum fibre stress is

$$\sigma_{max} = \frac{Mh}{2I} \qquad (13)$$

and comparing this with equation (5) shows that

$$(\dot{\sigma}_{max})_{SS} = \sigma_{max}(\frac{2n+1}{3n}) \tag{14}$$

Therefore

$$\dot{e}_{max} = \pm 4k \left[\sigma_{max}(\frac{2n+1}{3n})\right]^n \tag{15}$$

Thus a plot of log $\dot{e}$ versus log σ_{max} (σ_{max} being the initial maximum elastic stress) should yield a straight line of slope n.

Hoff suggested [19] that the creep expression could be written as

$$\dot{e} = f(\sigma) \, e^{-Q/RT} \tag{16}$$

Therefore combining equations (4) and (15) we get

$$\dot{e} = C \left[\sigma_{max} (\frac{2n+1}{3n})\right]^n \exp(-Q/RT) \tag{17}$$

where C combines constants.

B.   Materials, Analytical and Preparative Methods

1.   Uranium Dioxide

(a)   Polycrystalline:

Specimens of this material were obtained from sintered pellets, like those used as reactor fuel, supplied by Atomic Energy of Canada. The density was 96 per cent of theoretical (10.96 g/cc) and the grain size averaged 6 microns. The spectrographic analysis is given in Table I.

TABLE I

ANALYSIS OF URANIUM DIOXIDE USED IN THIS INVESTIGATION

ELEMENT	POLYCRYSTAL	SINGLE CRYSTAL		
	ppm	#6 ppm	#15 ppm	#16 ppm
Ag	-	-	-	-
Al	10	2	10	15
Au	-	-	-	-
B	2	-	-	-
Ba	-	-	-	-
Be	-	-	-	-
Bi	-	-	-	-
Ca	35	15	15	20
Cd	-	-	-	-
Cr	5	-	3	3
Cu	20	-	-	-
Fe	40	6	10	10
Mg	15	-	-	-
Mn	2	-	-	-
Mo	-	35	-	-
Na	150	nd	nd	nd
Ni	20	-	-	-
Pb	3	-	-	-
Si	9	5	-	2
Sn	-	-	-	-
Ti	1	2	1	1
V	-	-	-	-
W	-	6	-	-
Y	-	-	-	-
Zn	3	1	2	2
Zr	-	-	10	7

Spectrographic analysis by AECL Chalk River. Bar (-) indicates looked for but not detected.

(b) Single crystals:

Initially it had been hoped to grow single crystals by a floating-zone technique using either induction or resistance heating. However, considerable experimental difficulty was encountered because of the refractory nature of uranium dioxide. (See Appendix III.)

Single crystals, however, are available commercially from at least two sources. Spencer Chemical Company, Kansas City, Mo., will supply "...crystals of UO_2 of at least 3/16 inch in diameter, but it should be noted that this is a crystalline [sic] material and not necessarily single crystals". Material of this size range would be too small for the type of bend test specimen used in this investigation. The second source, Norton Company, Chippewa, Ontario, however, supplied rather large single crystals of UO_2, some of which were over 2 inches long and an inch in diameter. The fusion by Norton Company is carried out in an electric arc furnace with graphite electrodes, yielding 800-1000 lbs of polycrystalline product from 3/4 of a ton of raw material.[20] The polycrystalline mass is broken up and large grains (single crystals) are found in certain locations of the pig.

The sample crystal received from Norton Company was examined and found to be satisfactory for creep testing. On the basis of this, a large quantity was ordered. The crystals subsequently received appeared to have a rather dull mottled surface, were difficult to cut without cracking, and, on examination under the microscope, were found to have a large quantity of two-phase inclusions as shown in Figure 3.
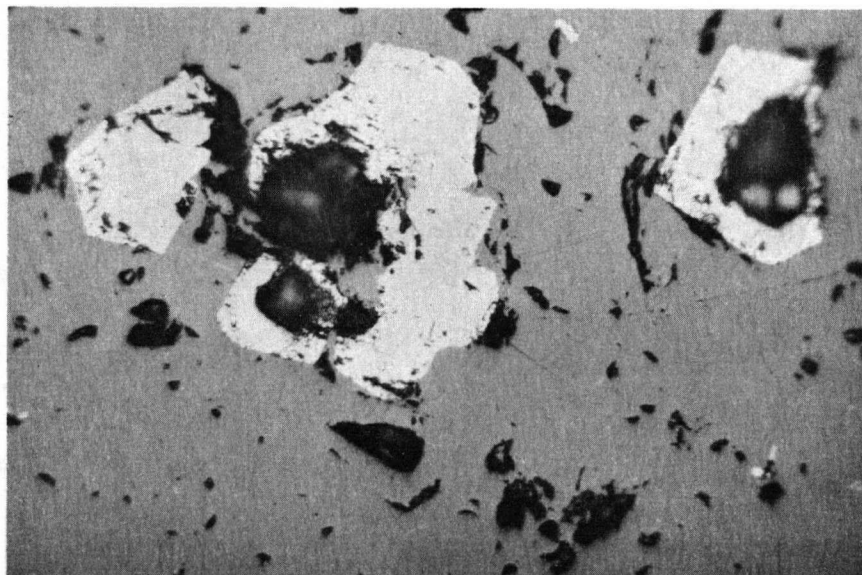
Figure 3   First batch of fused uranium dioxide, showing the
two-phase inclusions (480X)

These inclusions were qualitatively identified by X-ray diffraction
to be free uranium metal and uranium mononitride. The analysis is shown
in the column labelled #6 of Table I.

The second lot was found to be satisfactory in all respects:
the general appearance was much cleaner, it cut easily and no inclusions
could be observed (See Figure 4). The spectrographic analysis of crystals
#15 and #16 are in Table I. The supplier's analysis is

$$O/U \quad = 1.995 - 2.03$$
$$\text{Carbon} \quad = 0.01\% \text{ max.}$$
$$\text{Nitrogen} = 0.10\% \text{ max.}$$
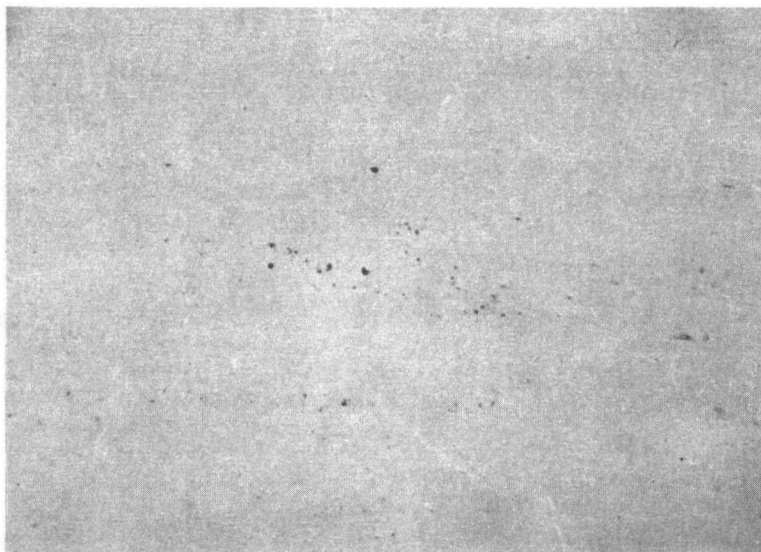
Figure 4   Second batch of fused uranium dioxide
           (480X)

2. Analytical Methods

Densities of the various specimens were determined by measuring
the weight loss of the specimen on immersion in carbon tetrachloride.

Stoichiometry was determined by measuring the weight-loss on
annealing in dry hydrogen for at least one hour at 1000°C. The hydrogen
was first passed through palladinized catalyst, then through a tube of
silica gel at room temperature, and finally through another tube of silica
gel immersed in liquid nitrogen to remove the last traces of moisture. As
a further precaution the specimens were quenched from 1000°C to room temp-
erature by pulling the boat containing them from the hot zone to the cool

end of the tube.

Orientations were determined by the standard technique of Laue back reflection.[21] The specimen was positioned with the major axis vertical so that the incident beam was parallel to the shortest dimension of the specimen. With a specimen-to-film distance of 3 cm and unfiltered molybdenum radiation (40kV, 10 ma) an exposure of 10 minutes was needed.

3. Specimen Preparation

The large as-received crystals were mounted in Plaster of Paris and cut into slabs of two to three mm in thickness in a direction that would yield slabs of maximum length. The slabs were mounted on transite with water-glass for cutting into bars in a direction that would yield the greatest number of specimens as shown in Figure 5.

Figure 5   Slabs and rough-cut specimens of fused
uranium dioxide

The as-cut bars were approximately two mm by three mm and 25 mm in length. All cutting was done with a diamond abrasive wheel (Felker-Di-Met) using water as coolant.

The bars were then ground to a thickness of about 1.8 mm using a slurry of 600 mesh alundum in dilute water-soluble coolant on a cast-iron lap. The final width of about 2.75 mm and final length of 22.5 mm were accomplished in the same manner.

Polishing of the surfaces was carried out in the following sequence: first 2/0 and 4/0 carborundum paper with kerosene as dust suppressor, followed by one-micron diamond paste on silk-covered glass. All specimens were given the same polish in order to hold surface conditions constant.

All specimens, separated by bubbled alumina, were placed in two alumina boats and heated for ten hours at 1600°C in a hydrogen atmosphere. Cooling of the furnace took 36 hours with the maximum cooling rate of 150°C per hour occurring in the first hour.

For metallographic examination of any surface the same procedure as described above is used, followed by $\frac{1}{4}$ micron diamond paste. The final polish was achieved by using a dilute slurry of "Linde B" alumina in 30% hydrogen peroxide on Beuhler "Microcloth". Surfaces were etched by immersion in freshly prepared solution of 30% hydrogen peroxide and concentrated sulphuric acid in the ratio of 9:1 respectively, for 10 to 30 seconds.

VI   EXPERIMENTAL PROCEDURE AND DATA

A.   Bend Creep Machine

1. Furnace and Temperature Control

The furnace consisted of four vertically mounted "Globar" resistance elements surrounded by refractories enclosed in a sheet metal container on the vertical sides and "Transite" on the upper and lower ends. The temperature was measured by a platinum-platinum + 10% rhodium thermocouple enclosed in an alumina protection tube which isolated the thermocouple from the hydrogen atmosphere. The thermocouple was checked periodically against another relatively little-used thermocouple and millivoltmeter which in turn had been calibrated at the melting point of lead (327°C). The thermocouple signal was fed, through temperature - compensating leads, to a Wheelco Model 402 indicator - controller (serial #95K3600), which maintained the temperature within $\pm\ 3^\circ$.

2. Creep Apparatus

The creep apparatus is illustrated in Figure 6. It consisted essentially of: a notched tube for supporting the bend specimen; a concentric loading tube with a chamfered inner surface at the tip, which applied two equal loads at equal distances from the centre of the beam; and, at the centre of the loading tube, a deflection rod, with sapphire tip, which transmitted the centerpoint deflection to the transducer and dial gauge. The latter two devices were attached to the loading tube so that the deflection is measured relative to the point of load application. Another tube concentric with and outside of the support tube and sealed at the ends permitted the use of a controlled atmosphere. The flexible seals for the loading tube and deflection rod were made from portions of toy balloons.
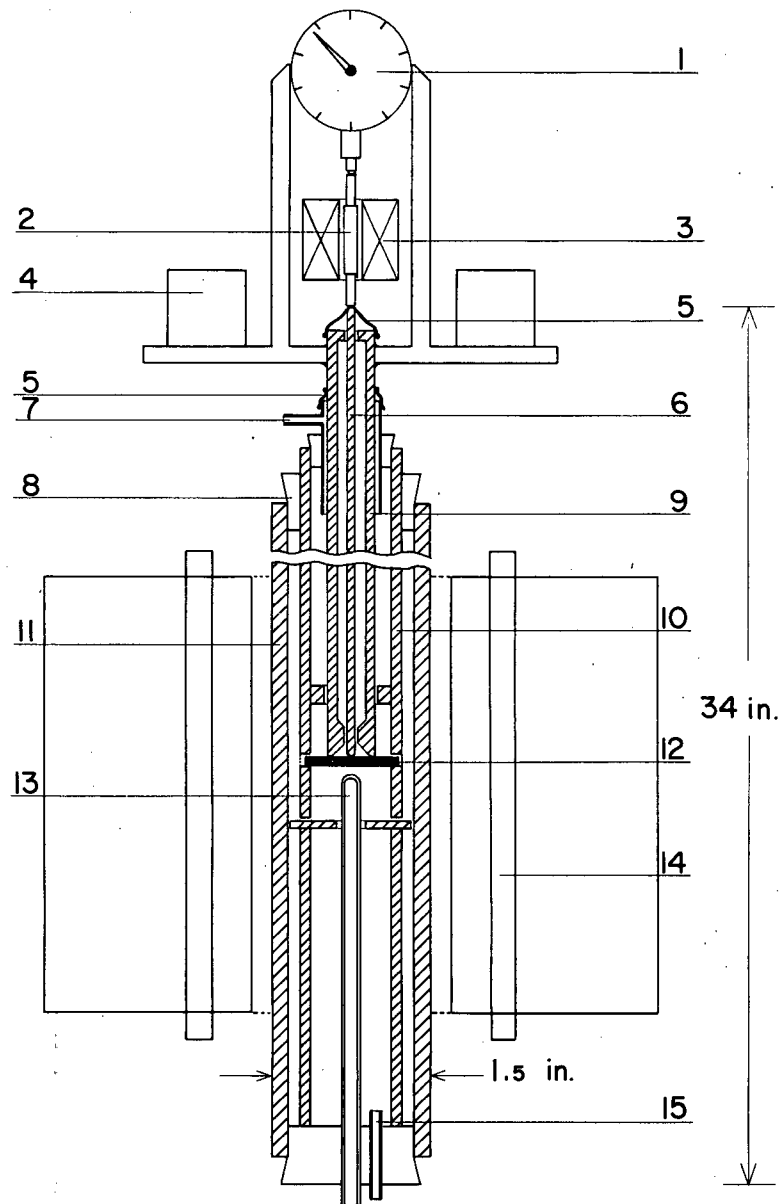
Figure 6   Schematic of Creep Apparatus

1	Dial Gauge	8	Rubber stopper
2	Iron core	9	Loading tube*
3	Transducer	10	Support tube*
4	Weight	11	Furnace tube
5	Flexible seal	12	Specimen
6	Deflection rod*	13	Thermocouple protection tube*
7	Gas inlet	14	Globar resistance element
		15	Gas outlet

*   "Purox" recrystallized alumina

The weights necessary to provide the desired load consisted of two small containers of test-lead whose total weight equalled the difference of the calculated load minus the sum of the weight of the loading tube and all the devices attached thereto.

The creep runs were performed with a hydrogen atmosphere purified by a palladinized catalyst and magnesium perchlorate dryer.

3. Measuring Devices

The vertical movements of the deflection rod were transmitted to the iron-core of a linear variable-impedance transducer, which in turn sent a voltage change proportional to the amount of vertical movement of the core, to a direct reading measuring bridge (Philips PR-9300, Serial #L0654) as shown in Figure 7. Continuous plotting of deflection with time


```
                                                    Transducer

   ┌──────────────┐        ┌──────────────┐
   │    Chart     │<-------│    Bridge     │<------  ▯ ▯
   │   Recorder   │        ├──────────────┤
   │              │        │  Oscillator   │------>
   └──────────────┘        └──────────────┘
     Philips                 Philips
     PR 2210/21              PR·9300
```
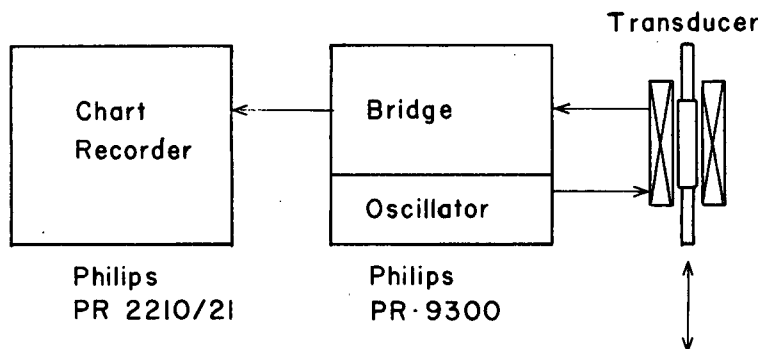
Figure 7   Diagram of electrical system

was obtained by connecting the output of the bridge to a strip-chart recorder (Philips PR2210 A/21, Serial #D1763). Both the bridge and recorder were powered through a constant voltage transformer to minimize

the effect of line voltage fluctuations.

The dial gauge (R.S. Starrett Company, No. 656-611) was used to calibrate the continuous plot by taking readings at various time intervals.

The general arrangement of the bend creep machine is shown in Figure 8.
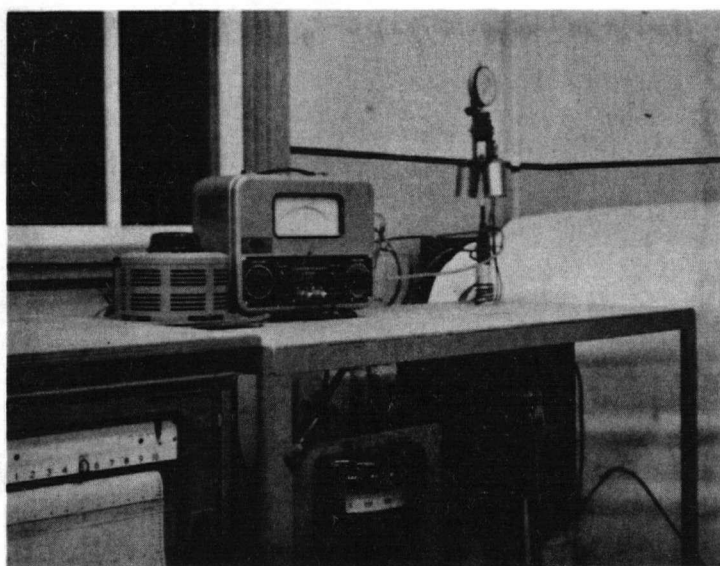
Figure 8   Bend creep machine

B.   Procedure

1. Constant Load, Constant Temperature

The prepared specimen was inserted into the slot of the support tube and the latter carefully placed inside the furnace tube. The complete loading assembly was then lowered to within a fraction of an inch of the specimen, as indicated by the deflection rod which was placed in contact with the centre of the beam. Therefore, the beam was never subjected to the weight of the loading assembly (1660 gms) but

only to the weight of the deflection rod during the warmup period. The whole assembly was checked for leaks, and then flushed with hydrogen before turning on the power to the furnace.

Not less than one hour after the desired temperature had been reached (to allow the furnace to come to temperature equilibrium) the load was slowly applied by lowering the loading tube, and the zero-point reading taken on the dial gauge. Further readings were taken on the dial-gauge at intervals to calibrate the chart. A total of four single-crystal specimens were tested in this manner, numbers 4, 3, 8 and 9, at 1400°C and at a load calculated to yield a maximum elastic fibre stress of 5000 psi (see Appendix II for details).

2. Constant Load, Variable Temperature

The initial procedure was as described in section 1 above, and the initial conditions were always 1400°C and 5000 psi. However, once steady-state creep had been established, the temperature was raised or lowered to a new value. The time taken for the change was always less than 15 minutes. Temperatures chosen were 1340, 1360, 1380 and 1420°C as well as 1400°C. Three specimens were tested in this manner: numbers 5, 15 and 16.

3. Variable Load, Constant Temperature

Again the initial procedure was as described above (except that the weights were added after the loading tube was lowered), but in this case, the load was changed by adding or subtracting the necessary weights to vary the maximum fibre stress from 5000 to 6000, 6000 to 7000, and 7000 to 5000 psi, all at 1400°C. One specimen only was tested in this manner, number 17.

C.   Results

1. Stoichiometry

The O/U ratio at the test temperature will be determined by the partial pressure of oxygen in the system. See Appendix IV for an estimate of the ratio.

Ratios were determined, however, on a few specimens:

TABLE II		
	O/U Ratio $\pm$ .002	
Sample	1	2
As received	2.000	2.004
Annealed	2.009	2.000
After creep	2.000	

2. Density

Densities of the samples taken were all greater than 99% of theoretical density (10.968 gm/cc); three are shown in Table III.

TABLE III	Densities		
	gm/cc $\pm$ 0.005		
Sample	1	2	3
As received	10.905	10.958	10.895
Annealed	10.956	10.974	10.931

3. Orientations

A typical Laue X-ray is shown in Figure 9. The orientation of the pole of the major axis of each specimen used is shown in the insert
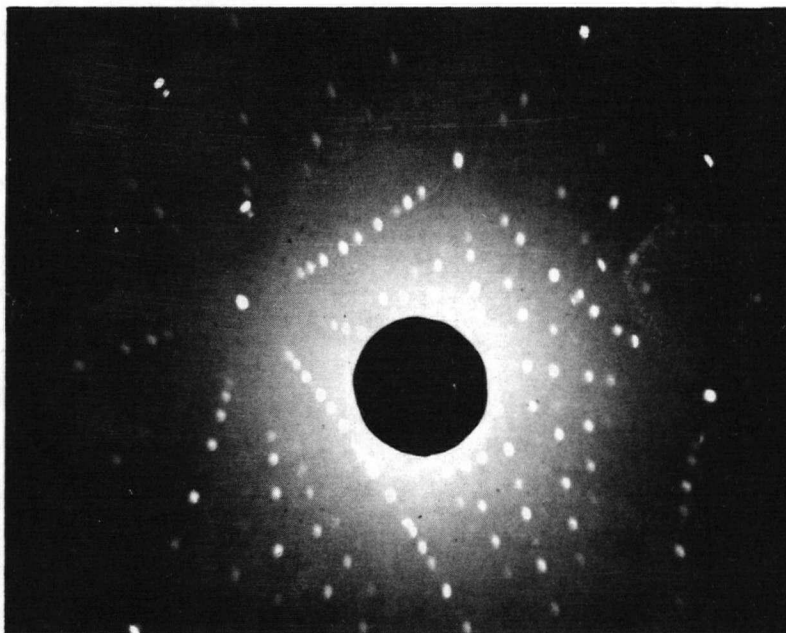
Figure 9   Typical Laue X-ray of uranium dioxide
single crystal

in Figure 16, with an estimated accuracy of $\pm 2^{\circ}$.

The (111) standard projection is used. In two cases, split
spots were observed, but repeated attempts could not reproduce this
effect in either case.

4. Constant Load - Constant Temperature

(a) Polycrystal:

Three polycrystalline specimens were deformed in four-
point bending and a representative deflection curve for one is shown in
Figure 10, for comparison with the single-crystal curves. Tertiary
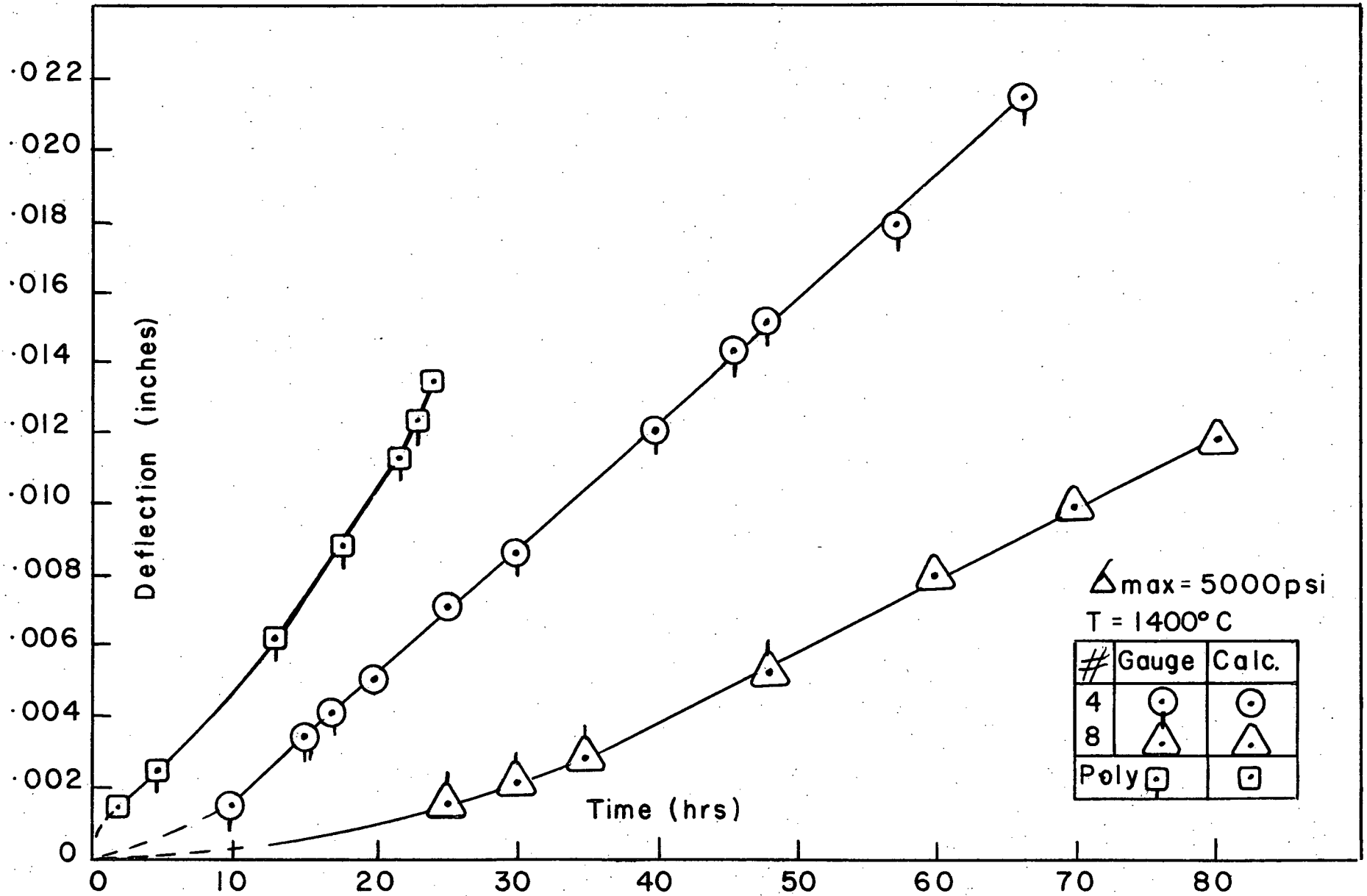
Figure 10.   Constant load — Constant temperature

creep always began after a deflection of about 0.01 inches, and cracks could be observed on the surface of the bar.

(b) Single crystals

The deflection curves of two of the four tested in this manner are shown in Figure 10, and the actual numbers used to calculate the deflection rates are given in Appendix V. The curves were not reproducible in the initial region because of the method of loading used, the difficulty in obtaining an exact zero-point reading on the gauge, and because some settling and digging-in of the loading tube occurred. The four-point bending resulted in deformation taking place over a greater length of the beam, as compared to three-point bending, (See Figure 11), but the same degree of uniformity was not obtained in all cases. Therefore, no absolute values of strain are available. Thus, only steady-state deflection rates and strain rates (calculated as shown in Appendix V) are reported.

No tertiary creep was observed in any runs, which were terminated before the specimen fell out of the support tube; and although some rather large deflections were obtained, no cracking whatsoever was observable.

Specimens which had a metallographic polish on one edge before deformation were examined after creep. These showed very faint lines on both sides of, but inclined to, the neutral axis and not extending through the neutral axis. These lines, which could be removed by polishing, are shown in Figures 12 and 13. The same lines were looked for but not observed on the upper and lower surfaces.
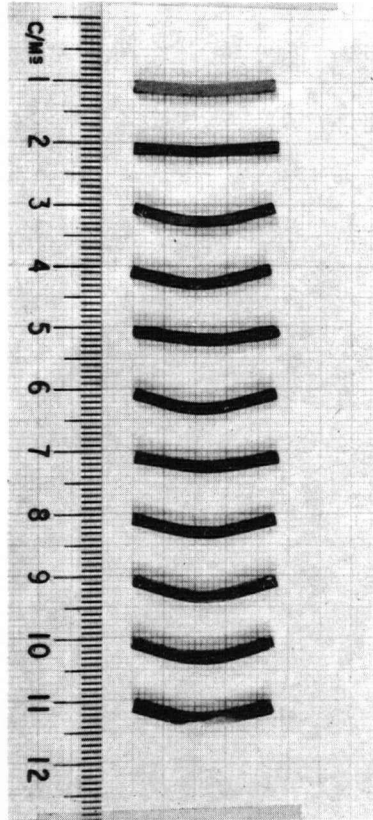
Figure 11   Plastically deformed uranium dioxide

1	Three-point loading	-	polycrystalline
2	Three-point loading	-	single crystal
3	Four-point loading	-	polycrystalline
4	Four-point loading	-	crystal #4
5	Four-point loading	-	crystal #3
6	Four-point loading	-	crystal #5
7	Four-point loading	-	crystal #8
8	Four-point loading	-	crystal #9
9	Four-point loading	-	crystal #16
10	Four-point loading	-	crystal #17
11	Four-point loading	-	crystal #15
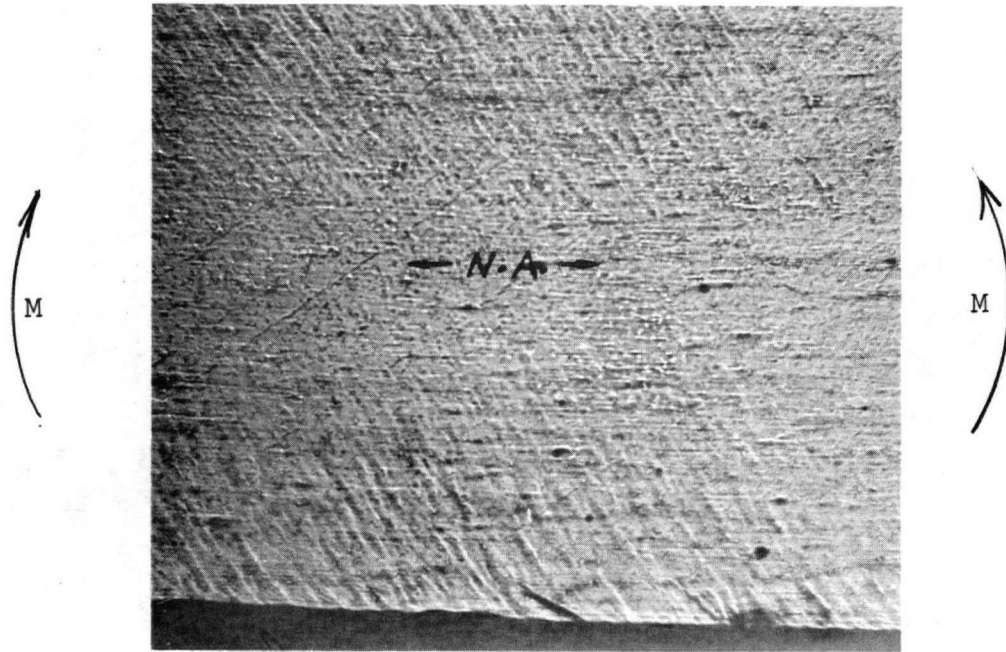
Figure 12   Edge view of specimen showing slip
lines on both sides of neutral axis
(60X)
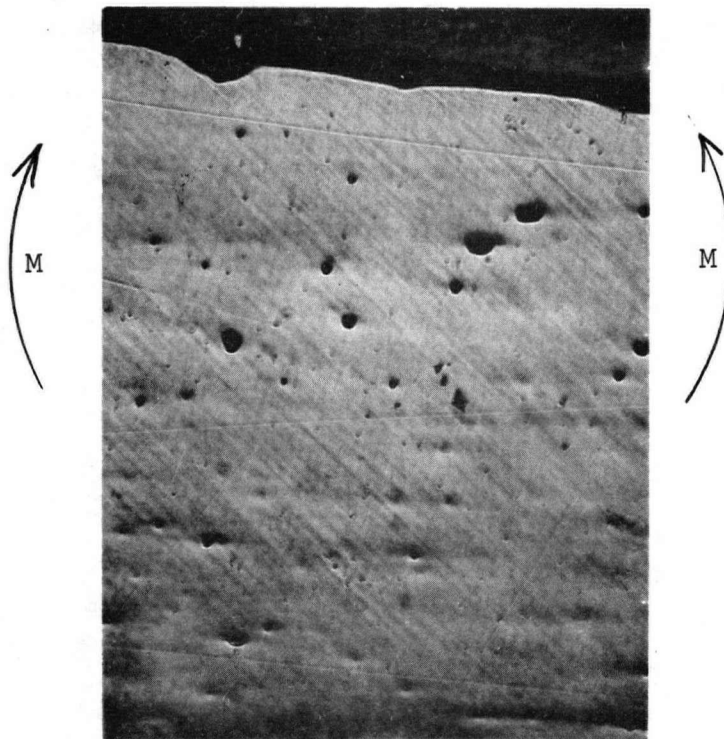
Figure 13   Edge view of slip lines at compression
surface. Pits are polishing artifacts.
(75X)

5. Constant Load, Variable Temperature

From the above results it was then assumed that once steady-state stress conditions had been obtained, they would prevail over relatively long times. Thus, it was possible to vary the temperature, without otherwise disturbing the system, to examine the effect of temperature on the rates. The results obtained are again given in Appendix V, and two of the three curves are plotted in Figure 14.

6. Variable Load, Constant Temperature

In this case the initial conditions again were 1400°C and a load calculated for a σ_{max} of 5000 psi. Steady-state creep was established as shown in Figure 15, then additional weight was added to increase the stress. This was done for two increases, and finally weight was removed to return to the original condition. The initial and final rates at 5000 psi were essentially the same, as shown in Appendix V.

7. Sources of Errors in the Results

(a) Temperature

Through the use of a relatively little-used thermocouple, assumed to be constant with time, the temperatures were reproducible to $\pm 5^{\circ}$; however, this reference thermocouple was not calibrated over the range of temperatures used in this investigation.

(b) Resolved shear stress

This calculation involved three linear measurements and two weight measurements giving an estimated maximum error of $\pm 10\%$, but this is overshadowed by the effect of the $\pm 2^{\circ}$ accuracy of the orientation determination.

Figure 14. Constant load — Variable Temperature
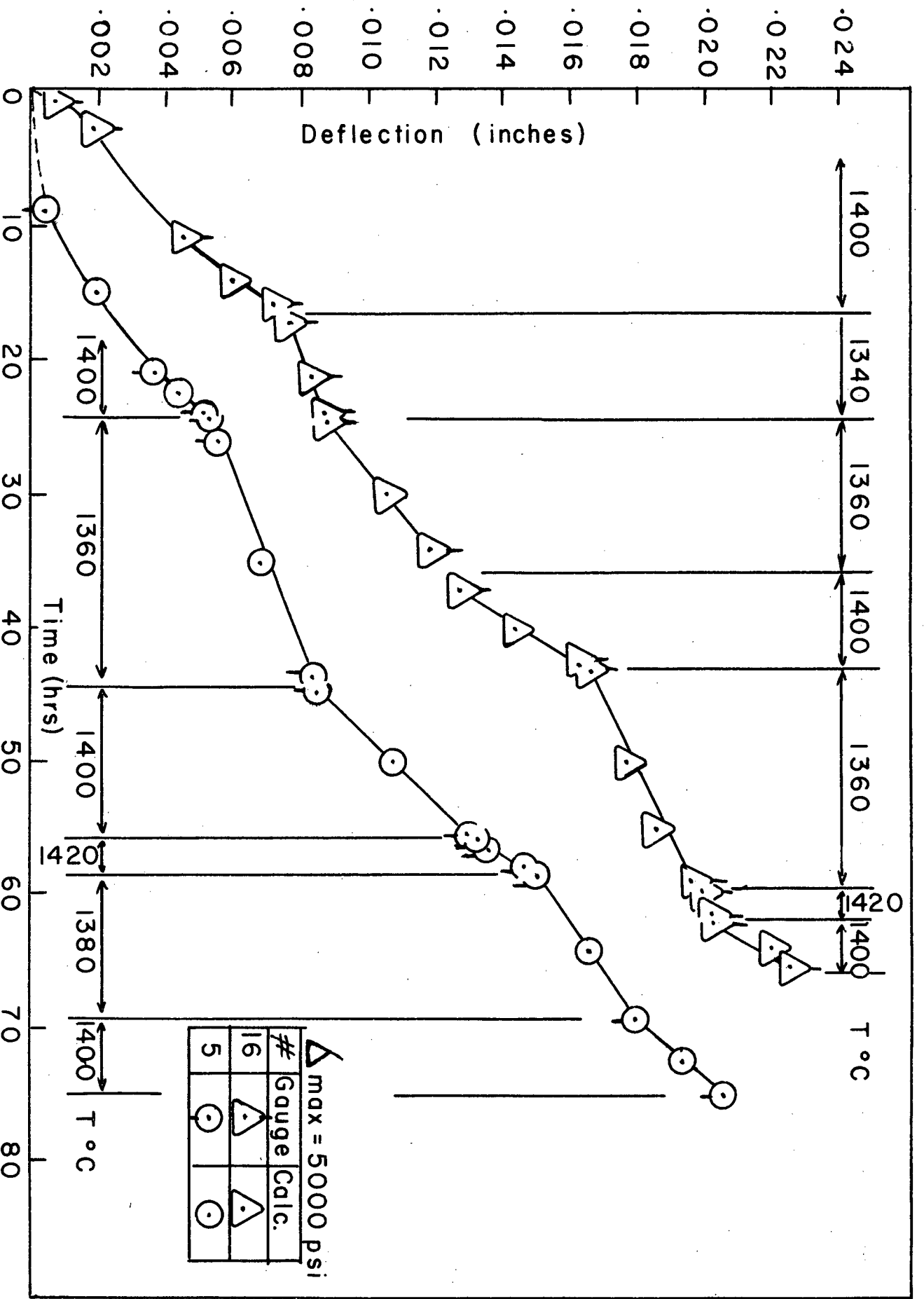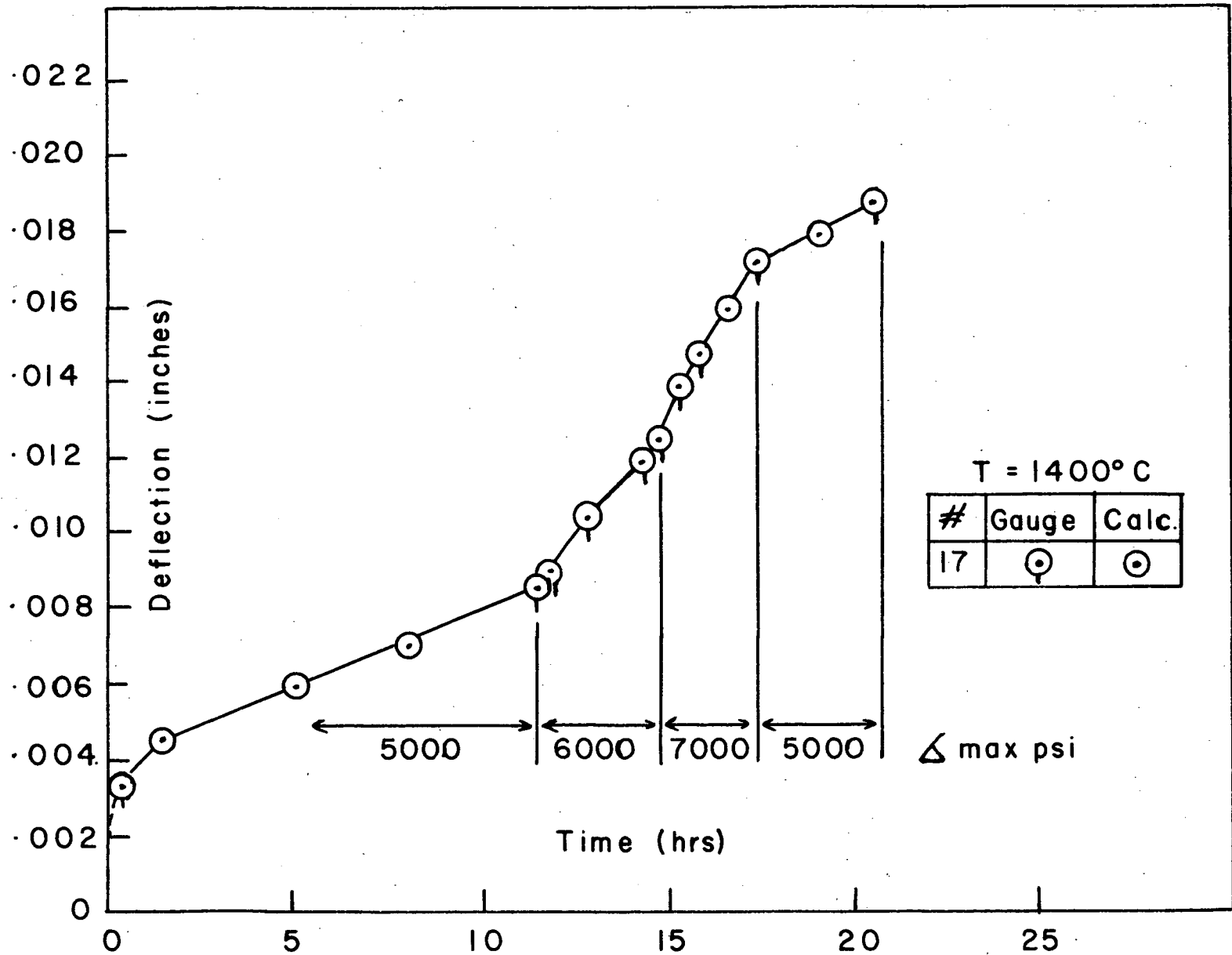
Figure 15.   Variable load — Constant Temperature

(c)   Others

For reasons given in section 4(b) above, no absolute values of strain are available. It should be pointed out as well that friction at the support points has been neglected. This would have the effect of superimposing a tensile stress on the bent specimens. Ideally at least one support point should be a roller support. Therefore stresses will be reported as the initial maximum fibre stress. (See Appendix II for analysis of stress redistribution.)

However, all runs were performed in the same manner and thus can be related one to the other by slopes as is done in section VII. One must be cautious, however, in drawing conclusions from values of intercepts.

VII   ANALYSIS AND INTERPRETATION

A. Stress Dependence

With all external variables held constant, the steady-state rates varied by a factor of five. Thus the more or less random orientations of the specimens must be determining the rates. The obvious approach is to calculate the maximum resolved shear stress and plot the data according to equation 15, on log-log scales. The calculations were performed as shown in Appendix VI and are plotted in Figure 16. The $\longmapsto$ lines delineate the range caused by the $^+_-2^\circ$ accuracy of the orientation determination. The solid line drawn through the points was calculated by the method of least squares, giving equal weight to all points, and has a slope of 3.4. Lines with slopes of four and three are drawn in for comparison. The two points which, if removed from the plot would then result in a line of about slope = 4, are #8 and #17 at 7000 psi. However, there is no obvious reason why those two should be any less reliable than other points, and therefore the slope appears to be less than four. This particular result may be of significance since Finnie and Heller[22] come to the conclusion, based on a theoretical derivation of Weertman[23] and on experimental work by Dorn[16] (both on steady-state creep at high temperatures and low stresses in fcc metals), that the stress exponent should be equal to four; that is

$$\dot{e}_c = K\sigma^4 \tag{18}$$

where $\dot{e}_c$ is the steady creep rate at high temperatures and low stresses, K is a material constant, and σ is the applied stress. Christy[24] points out that essentially the same ideas may be applied to ionic materials.
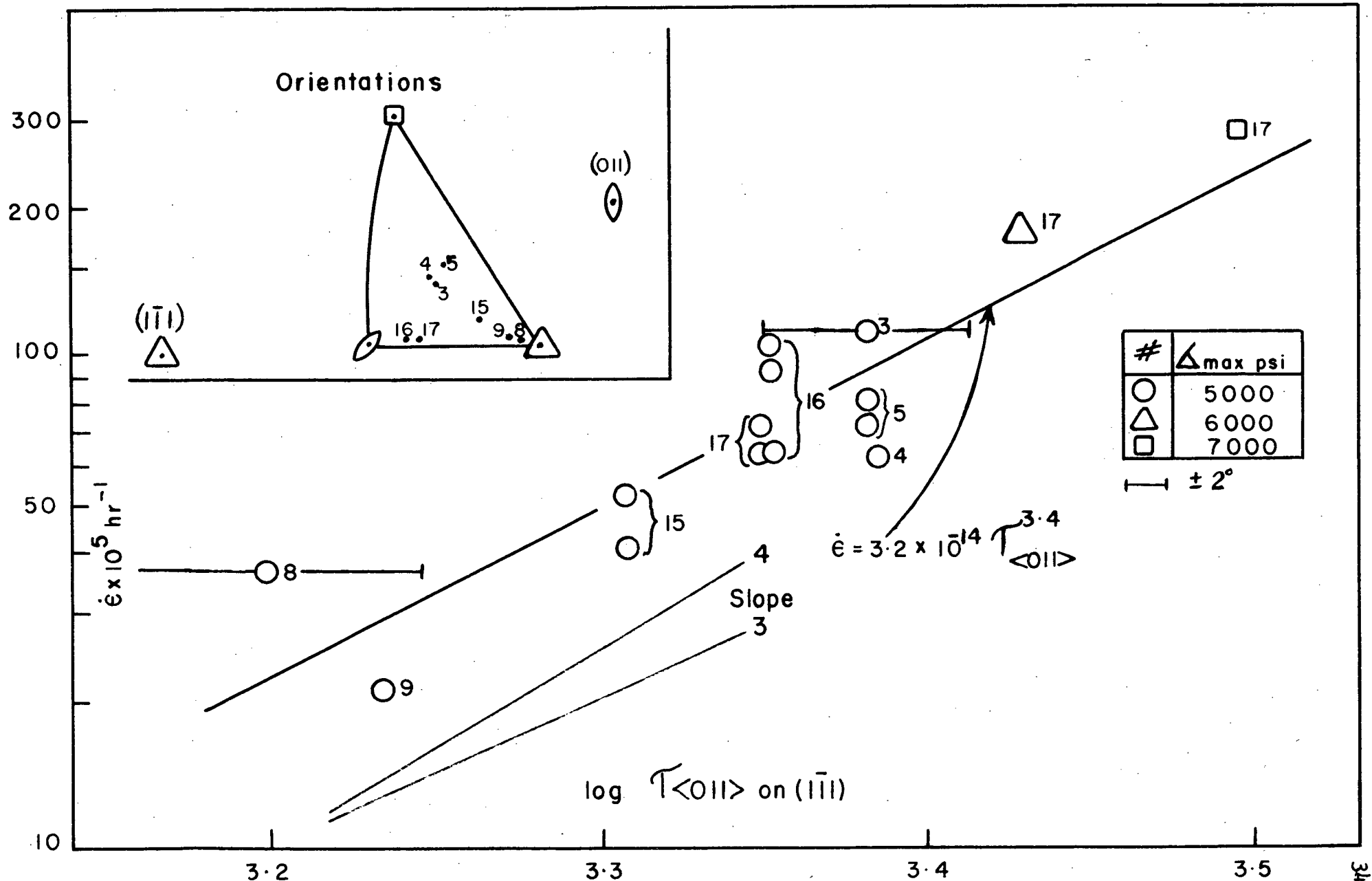
Figure 16.   Constant temperature

Thus, since n in this investigation appears to be less than four, the overall creep behaviour could involve, in addition to slip, some other processes.

B. Temperature Dependence

The steady-state rates when plotted as log rate versus reciprocal absolute temperature have the form shown in Figure 17, for the 5000 psi runs. The slopes of the three series #5, #15, and #16 were calculated independently by the method of least squares and were found to be within $\pm$ 20% of their mean value. Since $\pm$ 20% is not an unreasonable experimental error for an activation energy determination, it was assumed that the same activation energy was involved. Therefore the three curves were shifted vertically relative to the strain-rate axis so that the highest rate of each at 1400°C coincides with the thick-walled circle in Figure 18. The calculated activation energy from the slope of this line then, is 118 $\pm$ 23 kcal per mole. It must be emphasized again that this is an observed activation energy for the overall process. Nonetheless, it does lie at the upper end of the range reported[5] for the activation energy of self-diffusion of U^{4+} in stoichiometric UO_2 (95 to 120 kcal/mole).
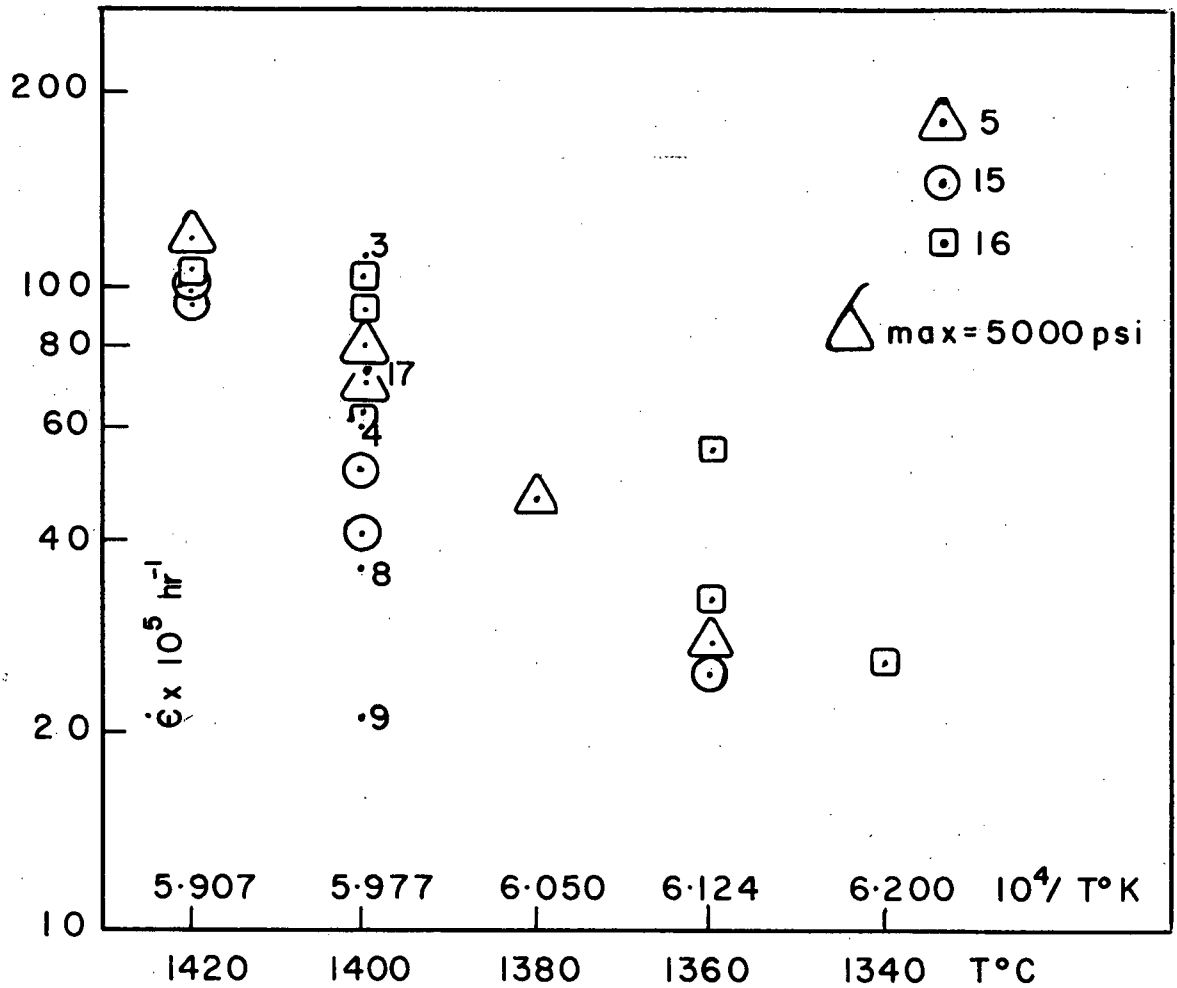
Figure 17   Arrhenius plot showing effect of
temperature on strain rate
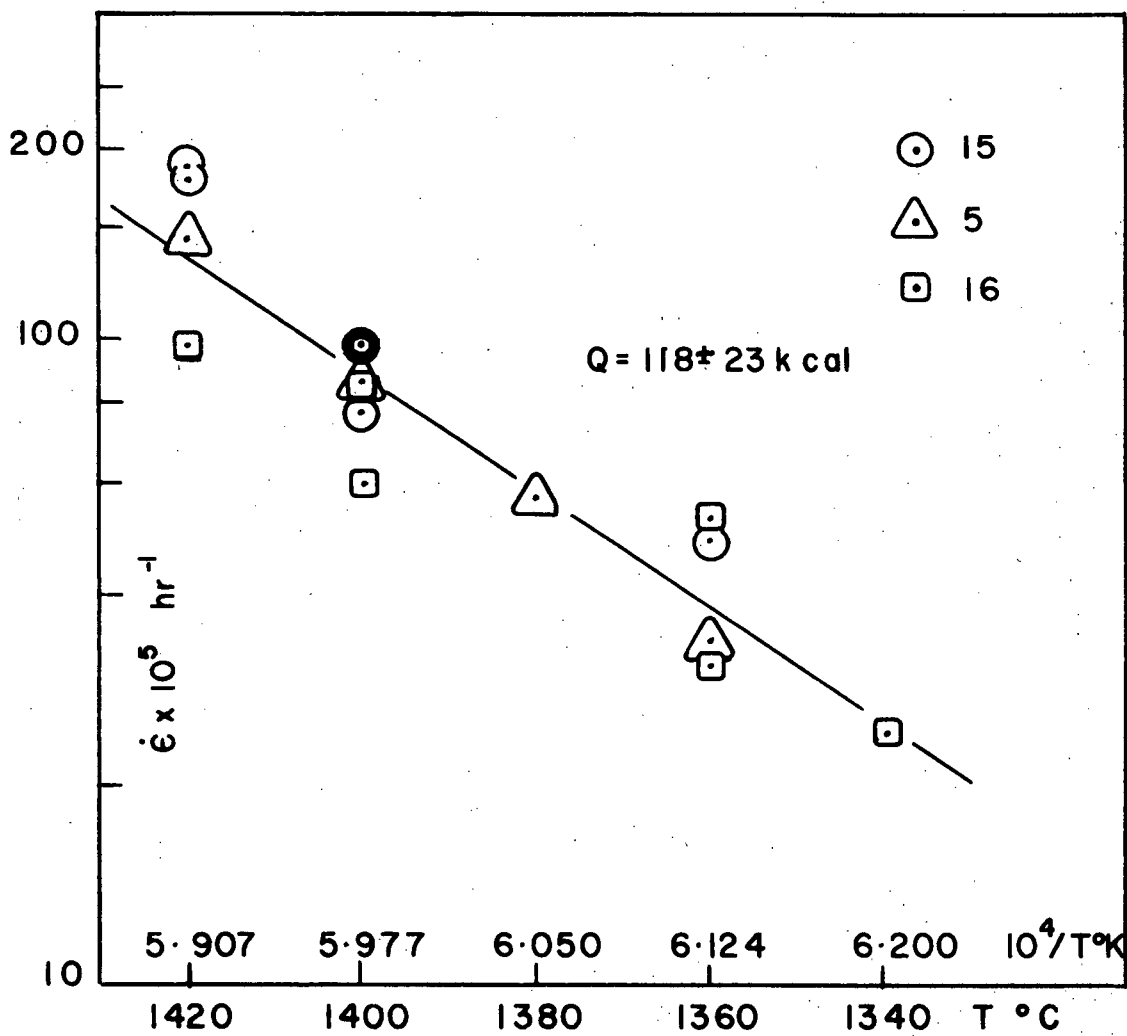
Figure 18   Shifted Arrhenius plot

VIII SUMMARY AND CONCLUSIONS

Stoichiometric single-crystals of randomly oriented uranium dioxide have been deformed in bending at low stresses and high temperatures to obtain steady-state creep rates. In the regions of stress and temperature examined, the results appear to fit the relationship:

$$\dot{e} = C(\sigma_{max})_{SS}^{n} \ \exp(-Q/RT)$$

where

$$\dot{e} = \text{steady-state creep rate}$$

$$(\sigma_{max})_{SS} = \gamma_{\langle 011 \rangle} = \text{resolved shear stress in } \langle 011 \rangle \text{ directions on } \{111\} \text{ planes}$$

$$Q = 118 \overset{+}{-} 23 \text{ kcal/mole}$$

$$C = \text{constant;} \quad \text{and } 3 < n < 4$$

Since faint slip lines were observed, slip must be involved in the overall process, but may not be the only process since n appears to be less than four.

IX   SUGGESTIONS FOR FUTURE RESEARCH

Certainly the first question to be answered is, does $n = 4$? More runs could be performed in the same ranges of temperature and stress to provide a statistically more satisfactory picture. The range of stresses then could naturally be extended to determine the limits of applicability of the assumed stress dependence.

If the four-point bending is continued, it is suggested that the loading be reversed so that the deflections (still relative to the two inner loads, which are now supports) can be measured relative to a stationary reference point at the lower end. The loads, at the ends of the beam, would be applied from the top.

Possibly dislocation densities and arrangements could be correlated with deformation by etching and X-ray techniques. Polygonization after creep deformation would be an interesting extension of this research.

APPENDIX I

THE URANIUM-OXYGEN SYSTEM

The uranium oxygen system is difficult to investigate owing
to the complex nature of the oxides formed and their extreme instability.
The results of various investigators are summarized in the phase diagram.
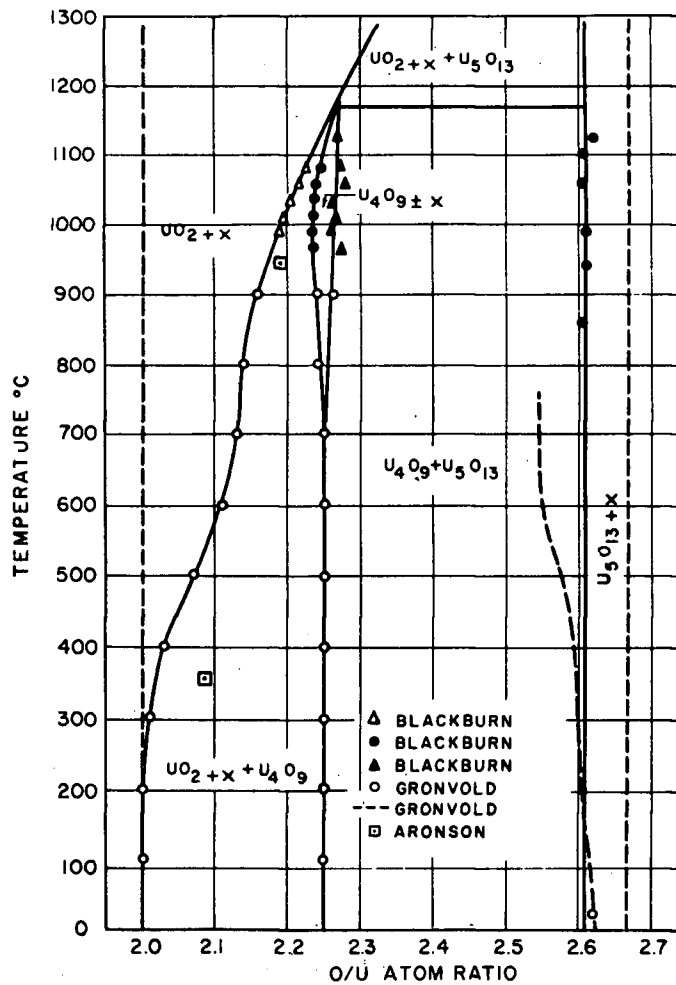
Figure AI   (after Seddon[24])

APPENDIX II

STRESSES IN BENDING

(1)   Three-point bending

A simply supported beam carrying a single concentrated load at the centre has a uniform shear stress along its length which changes sign at the centre. The bending moment varies linearly from the supports to a maximum at the centre. Thus the maximum elastic fibre stress

$$\sigma_{max} = \frac{3PL}{2bh^2} \tag{a}$$

occurs in the outer fibres at the centre of the beam. There are also contact stress concentrations in the fibres immediately below the applied load.

(2)   Four-point bending

A simply supported beam carrying two equal concentrated loads at equal distances from the supports has, in the centre section, zero shear stress, and constant bending moment as shown in Figure A II.1. The maximum elastic fibre stress

$$\sigma_{max} = \frac{Mh}{2I} = \frac{6Pd}{bh^2} \tag{b}$$

is distributed over the centre portion of the beam. The contact stresses again occur under the loads.
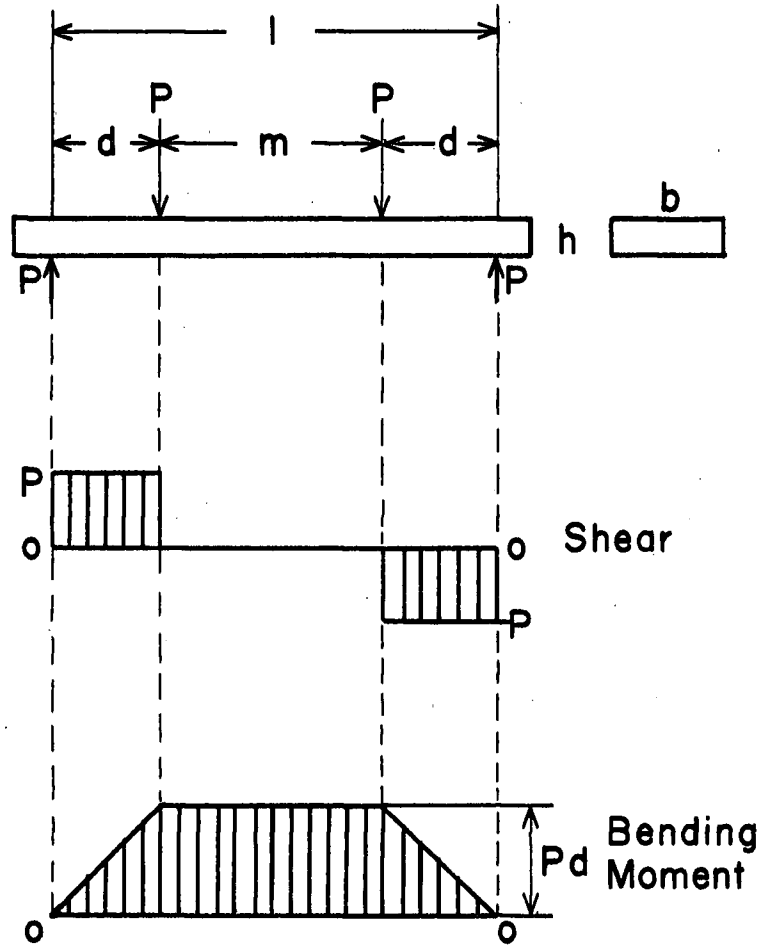
<u>Figure A.II.1</u>   Simple beam: two equal concentrated
loads at equal distances from supports
l = 18.65 mm
d = 4.375 mm
m = 10.00 mm

Thus the use of four-point bending, by distributing the maximum stresses uniformly along the centre length of the beam, actually results in the taking of a more representative sample of the material.

In this investigation the σ_{max} used was calculated from equation (b). That is, the total load to be used for a given beam was calculated using

$$W = 2P = \frac{(\sigma_{max})bh^2}{3d} \qquad (c)$$

The strain-rate was calculated using equation (11) of the text,

$$\dot{e}_{max} = \frac{4h}{m^2} \dot{y} \qquad (d)$$

which assumes the centre section is bent into a circular arc. If the value of m from figure A II.1, is substituted in equation (d), and if h is in millimetres and y in inches, then

$$\dot{e}_{max} = (1.015)h\,\dot{y} \qquad (e)$$

(3) Stress redistribution in beams undergoing creep

At the instant the load is applied, the beam undergoes an instantaneous elastic (and plastic) deflection. Initially before the beam has had time to creep the stress distribution is that given by elastic considerations and is shown as the straight line in Figure A II.2. The maximum fibre stress at the instant of loading will then be given by equations (a) or (b).
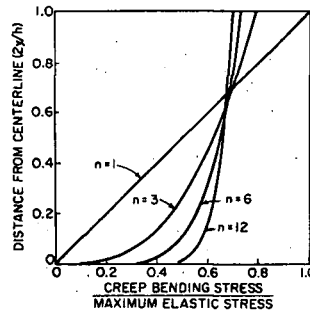
Figure A.II.2   Stress distribution in bending
                 (after Finnie and Heller[22])

Under the action of the applied stress the material of the

beam creeps. If the material deforms in a tensile test according to

equation (3) of the text

$$\dot{e} = K\sigma^n \tag{f}$$

the initial creep rates in the fibres in response to the linear elastic

stress distribution will not be proportional (if $n > 1$) to their distances

from the neutral axis. However, this situation would result in a

section that was not plane and in order to maintain a plane section the

stress in fibres near the neutral axis increases. Some time after the

load is applied, a state of stress distribution is reached in which the

strain rates in all fibres become proportional to their distances from

the neutral axis. This distribution is shown in Figure A.II.2. for

various n's.   Thus

$$(\sigma_{max})_{SS} = K(\sigma_{max})_{elastic} \tag{g}$$

where K is given by[18]

$$K = (\frac{2n+1}{3n}) \tag{h}$$

Assuming the creep law in equation (f).

APPENDIX III

GROWTH ATTEMPTS

During the initial stages of this research program attempts were
made to grow single crystals of UO_2 from the melt by using the floating zone
technique so successfully applied to many metals. However, UO_2 has a
melting point of $2800^{\circ}C$, a thermal conductivity of 0.003 cal/cm,sec,$^{\circ}C$,
an electrical conductivity of about $10^{-2}(\Omega\, cm)^{-1}$ at $500^{\circ}C$, and a vapour
pressure of about 1 mm Hg at its melting point. Thus it is a formidable
task indeed. As serious experimental work began, reports were received of
attempts of others to accomplish the same end, all more or less unsuccessful.
However some experimental attempts were made and these will be briefly outlined.

1) Induction heating: if UO_2 is heated above room temperature,
its electrical conductivity rapidly increases, and reports indicated that
UO_2 could be inductively heated above $1000^{\circ}C$. A one-turn coil of $\frac{1}{8}$" copper
plate was fabricated and connected to a Philips (output: 5KW, 800Kc)
induction unit. A rod of sintered UO_2, about $\frac{1}{4}$" square was enclosed in a
Vycor tube so that an argon atmosphere could be maintained, and was heated
with an oxy-gas torch to at least $1000^{\circ}C$. The tube containing the UO_2 was
lowered quickly into the powered coil. Several attempts were made, but no
heating effects were observed.

2) Resistance heating: Attempts were made to operate a narrow
tungsten filament, bent to the shape of a hair-pin, at temperatures close to
its melting point, to melt a narrow zone of UO_2 at the center of the circular
bend. The filament and rod of, again, sintered UO_2, were surrounded with
concentric molybdenum radiation shields and about 1000 watts of power were

needed to heat the filament to 3000°C. This furnace was enclosed in a

protective atmosphere of argon. During several runs, some melting of the

corners of the rod was observed. However, heat transfer considerations

indicated that the filament must be placed as close as possible to the rod

without touching it, and must be operated almost at its melting point.

Observations of the molten areas obtained showed that a very narrow zone only

(< 5mm) would be physically stable under the interactions of the surface

tension and gravity.

If resistance heating will ever be a feasible technique, it will

be with filaments of higher melting point materials (say TaC, or WC), since

a small increase in line voltage to the transformer supplying the high current-

low voltage power to the tungsten filament operated close to its melting

point will cause it to melt.

APPENDIX IV

STOICHIOMETRY AT TEMPERATURE

The oxygen pressure in equilibrium with UO_{2+x} at any temperature may be estimated from [25]

$$P_{O_2}(atm) = 76 \exp\left(\frac{-33000}{T^\circ K}\right) \exp\left(\frac{31x}{1-x}\right)$$

If the temperature is $1300^\circ C$ ($1573^\circ K$) and $x = 0$, then the pressure of oxygen in equilibrium with stoichiometric UO_2 is 5×10^{-8} atmospheres.

Assuming all oxygen is converted to water vapour by the palladinized catalyst, and taking a dew point of $-50^\circ C$ (for the anhydrone used, the dew point is $-80^\circ C$) which corresponds to $.00004$ atm water vapour, the partial pressure of oxygen may be estimated from

$$K = \frac{\left[P_{H_2}\right]\left[P_{O_2}\right]^{\frac{1}{2}}}{\left[P_{H_2O}\right]}$$

where K for $1300^\circ C = 4.91 \times 10^{-6} (atm)^{\frac{1}{2}}$.

Thus

$$P_{O_2} = \left(K\left[P_{H_2O}\right] / \left[P_{H_2}\right]\right)^2$$

$$= \left(\frac{(4.91 \times 10^{-6})(4 \times 10^{-5})}{1}\right)^2$$

$$\approx 20 \times 10^{-22} \text{ atm}$$

And even a dew point of $+50^\circ C$ gives a P_{O_2} of only 10^{-12} atm; therefore at temperatures used the uranium dioxide was stoichiometric.

APPENDIX V

SUMMARY OF EXPERIMENTAL RESULTS

In the following table, the symbols used are:

h	=	the height in millimeters
b	=	the width in millimeters
σ_m	=	max. fibre stress, psi (see Appendix II)
T	=	test temperature in $^\circ$C
d_1	=	deflection (gauge) inches x 10^5 at time t_1
t_1, t_2	=	time from beginning in hours
d_2	=	deflection (gauge) inches x 10^5 at time t_2
Δd	=	$d_2 - d_1$, inches x 10^5
Δt	=	$t_2 - t_1$, hours
$\dot{d}$	=	$\Delta d / \Delta t$, inches x 10^5 per hour
$\dot{e}$	=	$(1.015)(h)\dot{d}$, in/in x 10^5 per hour (see Appendix II)

In some cases it was not possible, due to the length of the runs, to obtain a gauge reading at the start (or finish) of a steady-state region and therefore the deflection had to be calculated using a chart calibration of 22.8 x 10^{-5} inches per division. Values obtained in this manner are marked *. The points plotted as "calc" in Figs. 10, 14, 15 were obtained the same way.

#	Origin	h	b	σ_m	T	d_1	t_1	d_2	t_2	Δd	Δt	$\mathring{d}$	$\mathring{e}$
4	N 15 C 02	1.82	2.76	5000	1400	349	15	2149	66	1700	51	33.3	61.5
3	N 15 C 03	1.85	2.65	"	"	365*	15	836	23	471	8	59.0	110
5	N 15 D 01	1.70	2.45	"	"	360	21	501	24	141	3	47.0	81.1
				"	1360	542	26	825	44	283	18	15.7	27.1
				"	1400	828	44.50	1283	55.50	455	11	41.4	71.4
				"	1420	1304	55.75	1459	58	155	2.25	69.0	119
				"	1380	1497	58.50	1788	69.25	291	10.75	27.0	46.6
				"	1400	1788	60.25	2055	75	267	5.75	46.5	80.3
8	N 16 B 01	1.80	2.72	"	"	288	35	1182*	80	894	45	19.9	36.4
9	N 16 B 02	1.76	2.45	"	"	125	26	347	44.75	222	18.75	11.9	21.0
16	N 20 B 02	1.65	3.25	"	"	445	11	719	16	274	5	54.8	91.9
				"	1340	763	17.25	867	24	104	6.75	15.4	25.8
				"	1360	867	24.25	1186*	34	319	9.50	33.6	56.2
				"	1400	1270	37	1626	42.75	356	5.75	62.0	104
				"	1360	1647	43	1957	59	310	16	19.4	32.5
				"	1420	1983	59.75	2080	61.50	93	1.50	62.0	104
				"	1400	2125	62	2248	65.25	123	3.25	37.8	63.4
17	N 21 A 02	1.75	3.05	"	"	458*	1.50	861	11.50	403	10	40.3	71.6
				6000	"	1050	12.75	1199	14.25	149	1.50	99.3	177
				7000	"	1482	15.75	1722	17.25	240	1.50	160	284
				5000	"	1722	17.25	1873	20.50	151	4.25	35.5	63.0
15	N 22 B 02	1.85	3.10	"	"	127	16	502	33.50	375	17.50	21.5	40.3
				"	1420	502	33.50	777	38.75	275	5.25	52.4	98.3
				"	1360	803	39	1038	56.50	235	17.50	13.4	25.2
				"	1400	1080	58.75	1370	69.25	290	10.50	27.6	51.8
				"	1420	1372	69.50	1435	70.75	63	1.25	50.4	94.5

APPENDIX VI

CALCULATION OF RESOLVED SHEAR STRESS

In the table below

λ is the great circle angle from [011] pole to the pole of the major axis

θ is the great circle angle from (1̄11) pole to the pole of the major axis

$$\tau = \sigma_{max} \cos \lambda \cos \theta$$

σ_{max} as defined in Appendix II

#	λ	$\cos\lambda$	θ	$\cos\theta$	$\cos\lambda\cos\theta$	$\tau\langle 011\rangle$	log τ	ė
15	38	.788	59	.515	.406	2030	3.308	40.3, 51.8
8	36	.809	67	.319	.316	1580	3.199	36.4
9	36	.809	65	.423	.342	1710	3.234	21.0
3	40	.766	51	.629	.482	2410	3.382	110.
4	41	.755	50	.643	.485	2425	3.385	61.5
5	37	.799	53	.602	.481	2400	3.381	81.1,71.4,80.3
16	52	.616	43	.731	.450	2250	3.352	91.9,104,63.4
17	50	.643	46	.695	.447	2235	3.349	71.6,63.0
						2680	3.428	177
						3120	3.495	284

XI REFERENCES

(1)   Gilman, J. J.,   Mechanical Properties of Ionic Crystals, in
                       Prog. in Ceram. Sci., J.E. Burke, ed., 1
                       (1961), 146.

(2)   Kingery, W.D.,   Property Measurements at High Temperatures,
                       (1959), 149.

(3)   Chang, R.,   High Temperature Creep and Anelastic Phenomena
                   in Polycrystalline Refractory Oxides, J.Nuc.Mat.,
                   2 (1959), 174.

(4)   Parr, N.L., et al., Preparation, Microstructure and Mechanical
                       Properties of Silicon Nitride, in Special Ceramics,
                       P. Popper, ed., (1960), 102.

(5)   Scott, R., Hall, A.R., and Williams, J., The Plastic Deformation
                       of Uranium Oxides Above 800°C, J. Nucl. Mat., 1
                       (1959), 39.

(6)   Wachtman, J.B.,   Creep of Crystalline Nonmetals, in Creep and
                       Recovery, ASM Trans., 49A (1957), 344.

(7)   Azaroff, L.V.,   Introduction to Solids (1960), 360.

(8)   Swanson, H.E. and Fuyot, R.K., Standard X-Ray Diffraction Powder
                       Patterns, NBS Circular 539, II (1953), 34.

(9)   Aronson, S., and Belle, J., Nonstoichiometry in Uranium Dioxide,
                       Jour. Chem.Phys., 29 (1958), 151.

(10)   Gronvold, F.,   High Temperature X-Ray Study of Uranium Oxides in
                       the UO_2 - U_3O_8 Region, J. Inorg. and Nuc. Chem.,
                       1 (1955), 357.

(11)   Anderson, J.S., et al., Decomposition of Uranium Dioxide at its
                       Melting Point, Nature, 26 Mar. (1960), 915.

(12)   Burdick, M.D., and Parker, H.S., Effect of Particle Size on Bulk
                       Density and Strength Properties of UO_2 Specimens,
                       J.Amer.Ceram.Soc., 39 (1956), 181.

(13)   Armstrong, W.M., Irvine, W., and Martinson, R., Creep Deformation
                       of Stoichiometric UO_2 , to be published in Jour. Nuc.
                       Materials.

(14)   Rapperport, E.J., and Huntress, A.M., Deformation Modes of Single
                       Crystal Uranium Dioxide from 700° to 1900°C, Nuclear
                       Metals Inc., NMI - 1242 (1960).

(15) Finnie, I.,   Stress Analysis in the Presence of Creep, Appl.
                       Mech. Rev., 13 (1960), 705.

(16) Dorn, J.E.,   The Spectrum of Activation Energies for Creep,
                       in Creep and Recovery, ASM Trans., 49A (1957), 255.

(17) Duckworth, W.H., Precise Tensile Properties of Ceramic Bodies,
                       Jour. Amer.Ceram. Soc., 34 (1951), 1.

(18) Timoshenko, S., Strength of Materials, Part II, (1956), 527.

(19) Hoff, N.J.,   Mechanics Applied to Creep Testing, SESA Proceed.,
                       XVII (1958), 1.

(20) Scott, J.J.,   Fused Uranium Oxide, paper delivered Amer.Ceram.Soc.,
                       Toronto (1961).

(21) Cullity, B.D.,   Elements of X-Ray Diffraction, (1956), 215.

(22) Finnie, I., and Heller, W.R., Creep of Engineering Materials,
                       (1959), 80.

(23) Weertman, J.,   Theory of Steady-State Creep Based on Dislocation
                       Climb, J.Appl.Phys., 26 (1955), 1213.

(24) Seddon, B.J.,   Uranium Ceramics Data Manual, UKAEA, DEG Report
                       120R (1960), 32.

(25) Webster, A.H., and Bright, N.F., The Effects of Furnace Atmosphere
                       on the Sintering Behaviour of Uranium Dioxide,
                       Department of Mines and Technical Surveys, Ottawa,
                       Research Report R2 (1958).